Available online at www.sciencedirect.com
ScienceDirect
Journal of Power Sources 184 (2008) 657–662
JOURNAL OF POWER SOURCES
www.elsevier.com/locate/jpowsour

Short communication

Preparation and electrochemical properties of Co–Si_3N_4 nanocomposites

S.M. Yao, K. Xi, G.R. Li, X.P. Gao *

Institute of New Energy Material Chemistry, Nankai University, Tianjin 300071, China

Received 26 December 2007; received in revised form 27 January 2008; accepted 29 January 2008
Available online 13 February 2008

Abstract

Cobalt nanoparticles on an amorphous Si_3N_4 matrix were synthesized by direct ball-milling of Co and Si_3N_4 powders for an improvement of their electrochemical performance. The microstructure, morphology and chemical state of the ball-milled Co–Si_3N_4 composites are characterized by X-ray diffraction (XRD), transmission electron microscopy (TEM) and X-ray photoelectron spectroscopy (XPS). The electrochemical performance of Co–Si_3N_4 composites was investigated by galvanostatic charge–discharge process and cyclic voltammetry (CV) technique. It is found that metallic Co nanoparticles of 10–20 nm in size are highly dispersed on the amorphous inactive Si_3N_4 matrix after the ball-milling. The composite with a Co/Si molar ratio of 2/1 shows the optimized electrochemical performance, including discharge capacity and cycle stability. The formation of Co nanoparticles with a good reaction activity is responsible for the discharge capacity of the composites. The reversible faradic reaction between Co and β-$Co(OH)_2$ is dominant for ball-milled Co–Si_3N_4 composite. The surface modification of the hydrogen storage $PrMg_{12}$–Ni composites using Co–Si_3N_4 composites can enhance the initial discharge capacity based on the hydrogen electrochemical oxidation and Co redox reaction.

Keywords: Ball-milling; Cobalt; Silica nitride; Electrochemical behavior; Oxidation; Reduction

1. Introduction

It is well known that cobalt has a wide application in various power sources, including Ni-metal hydride (Ni-MH) batteries, lithium ion batteries, proton exchange membrane fuel cells (PEMFCs) and solid oxide fuel cells (SOFCs) [1–4]. It is reported that hydrogen can be stored in crystalline Co powder and Co oxides in the form of CoH_X due to the phase transition from hcp-Co to fcc-Co during the charge process [5,6]. In recent years, extensive research has been focused on cobalt-based alloys as hydrogen storage electrode materials, such as Co–B, Co–P, Co–Si and MgNi–CoB [7–11], which are demonstrated to have a good electrochemical reversibility and large charge–discharge capacities. However, metallic Co is an active material being easily oxidized or corroded in air or electrolyte environments [12], so that insoluble and stable cobalt oxide films are formed on the surface of metal particles [13]. Particularly, it was reported that $Co(OH)_2$ underwent a quasi-reversible reduction to cobalt at potentials close to the hydrogen evolution reaction [14]. Electroless cobalt coatings on the surface of AB_5 hydrogen storage alloys were shown to have beneficial effects on the discharge capacity and cycle life due to the faradaic reaction in the Co/$Co(OH)_2$ couple [15,16]. Furthermore, the metallic cobalt in alkaline solution has different valence changes as the oxidation potential varied [17], and the conversion from Co to $Co(OH)_2$ occurs at the potential of −0.83 to −0.85 V (vs. Hg/HgO) [15]. The utilization of the metallic cobalt in the oxidation reaction is greatly determined by the particle size or dispersion of active materials. On the other hand, the amorphous structure is more effective for the enhanced utilization due to faster transport of active species as compared to crystalline materials [15].

Ball-milling is an efficient method for preparing well-dispersed nanoparticles, and the incorporation of inactive materials can effectively restrain the agglomeration of active nanomaterials. Hayashi et al. found that cobalt nanocrystals were completely isolated from each other by graphite-like carbon as the carbon layers, which can significantly reduce the exchange coupling between these nanocrystals [18]. The dual-phase composites consisted of active Si and inactive material

* Corresponding author. Tel.: +86 22 23500876; fax: +86 22 23500876.
E-mail address: xpgao@nankai.edu.cn (X.P. Gao).

0378-7753/$ – see front matter © 2008 Elsevier B.V. All rights reserved.
doi:10.1016/j.jpowsour.2008.01.077

such as Si–Si_3N_4 [19], showed improved electrochemical performance as anode materials for lithium ion batteries. This is due to the uniform distribution of active nanoparticles on the inactive matrix.

Silicon nitride (Si_3N_4) exhibits a good chemical stability and an electrochemical passivation in alkaline solution. In this work, the Co–Si_3N_4 composites are prepared via a ball-milling process and their electrochemical behaviors are investigated. In addition, the effect of the Co–Si_3N_4 composites as additives on the discharge capacity of $PrMg_{12}$ hydrogen storage alloy is also investigated.

2. Experimental

The Co–Si_3N_4 composites were prepared by direct ball-milling of cobalt powder (purity, 99%) and amorphous Si_3N_4 particles (from HeFei Kaier Nanometer Technology Development Co., Ltd.) using a planetary-type ball-miller. The weight ratio of balls to powder was set to be 20/1 and the ball-milling was conducted with a rotation rate of 580 rpm for 13 h under Ar atmosphere. All samples were characterized by X-ray diffraction (XRD, Rigaku D/max-2500). The morphology, microstructure and chemical state were investigated with transmission electron microscopy (TEM, FEI Tecnai 20) and X-ray photoelectron spectroscopy (XPS, Kratos Axis Ultra DLD).

The electrochemical measurements were carried out in a three-compartment cell. A sintered nickel electrode with a large capacity and an Hg/HgO electrode in 6 M KOH solution served as counter and reference electrodes, respectively. Electrodes were constructed through mixing as-prepared composites with carbonyl nickel powder in a weight ratio of 1:3. The mixture powder was pressed under 30 MPa into a small pellet of 10-mm diameter and 1.5-mm thickness. Charge–discharge cycle tests were performed using Land battery test instruments controlled by a computer. The negative electrodes were charged at a current density of 300 mA g^{-1} for 90 min, and then discharged to −0.6 V (vs. Hg/HgO) at the current density of 60 mA g^{-1} after resting for 5 min at room temperature. Cyclic voltammetry (CV) experiments were conducted using Zahner IM6e electrochemical workstation. The working electrodes for CV test were made by mixing active materials with polytetrafluoroethylene (PTFE) aqueous suspension, pasting the mixture on nickel foam and then dried in a vacuum drier before testing. The potential scan rate was set to be 0.2 mV s^{-1} and the initial potential was the steady value of the electrode in alkaline solution.

To investigate the electrochemical reaction mechanism, the microstructure of the ball-milled Co–Si_3N_4 composites after different cycles was measured by XRD. In order to avoid the influence of the Ni diffraction peaks, the electrodes for XRD measurement were prepared by mixing Co–Si_3N_4 powders, acetylene black and polytetrafluoroethylene at the weigh ratio of 10:2:1 into a paste, which was roll pressed to 0.15-mm thick film and then pressed onto a porous nickel mesh. After electrochemical cycles, the samples at different discharged and charged states for XRD measurements were washed with distilled water and ethanol, and dried in vacuum at 80 °C for 3 h.

The $PrMg_{12}$ alloy was synthesized through a molten-salt-cover-melting process by melting a stoichiometric mixture of metallic Pr and Mg as reported in our previous work [20]. The ingot was then pulverized to 200 mesh. The modification was conducted by further mechanical milling of the $PrMg_{12}$ alloy with 200 wt% of carbonyl nickel powder (255INCO) and Co–Si_3N_4 composite (14 wt%). The weight ratio of carbonyl nickel powders to the pulverized alloy was set as 2:1 (total mass of 6 g). The charge–discharge curves of $PrMg_{12}$–Ni–(Co–Si_3N_4) composite were performed in an alkaline solution. When the discharge capacity was calculated, only the $PrMg_{12}$–Ni composite was considered as the active material.

3. Results and discussion

Fig. 1 shows XRD patterns of ball-milled Co and Co–Si_3N_4 composites with different Co/Si molar ratios. The original Co powders have two structures of cubic structure (JCPDS 89-4307) and hexagonal structure (JCPDS 89-4308). All diffraction peaks of ball-milled Co and Co–Si_3N_4 composites are broadened and weakened, indicating the formation of nanocrystalline Co during the ball-milling process. It is also shown that there are no new phases, such as Si, Co–Si and Co–N, formed in the Co–Si_3N_4 composites or decomposed from Si_3N_4 particles during the ball-milling process.

Initial charge and discharge curves of Co–Si_3N_4 composites with different Co/Si molar ratios are presented in Fig. 2. It is noted that all samples can be discharged directly without a pre-charged process in the first cycle, corresponding to the electrochemical oxidation of Co into Co(II) in the absence of hydrogen atom in the lattice of alloy or metal, which are different from metal hydride electrodes. After the pre-charged process in the first cycle, the initial discharge capacities increase obviously for all samples. These oxidized species (as shown in XPS) on the surface of the Co–Si_3N_4 composite are first reduced to Co during the pre-charged process and subsequently also oxidized to $Co(OH)_2$, hence the increased capacity is obtained for

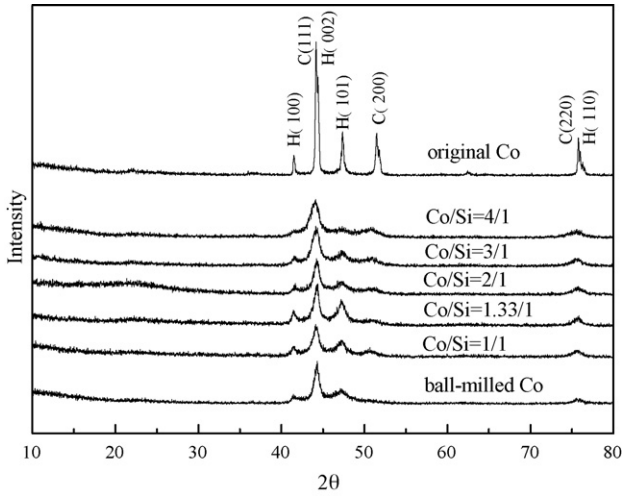

Fig. 1. XRD patterns of ball-milled Co and Co–Si_3N_4 composites with different Co/Si molar ratios.

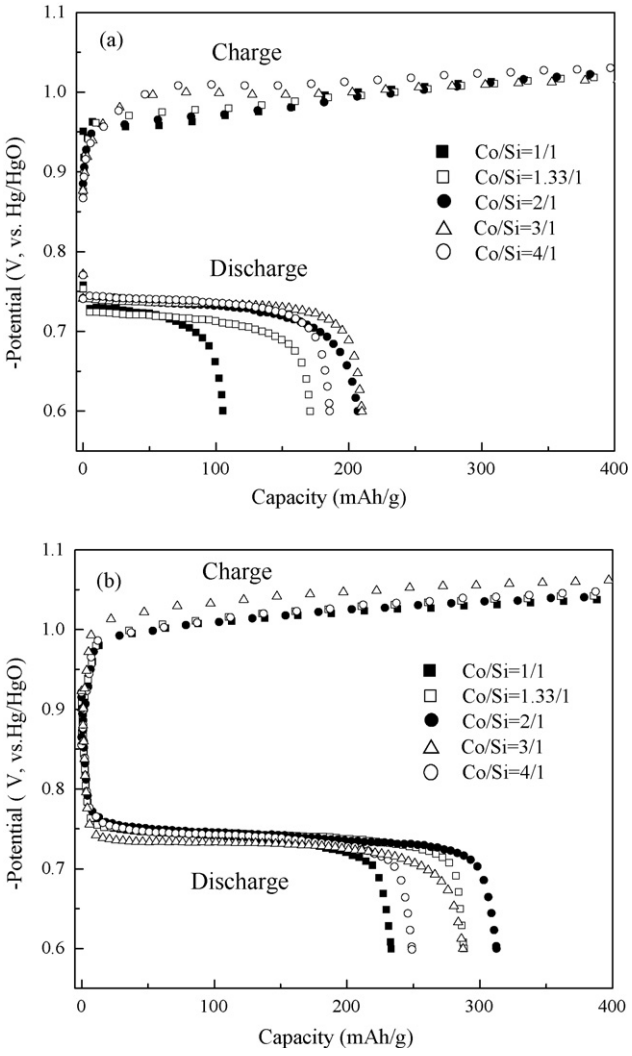

Fig. 2. Initial charge–discharge curves of Co–Si_3N_4 composites with different Co/Si molar ratios: (a) discharging directly in the first cycle and (b) charging directly in the first cycle.

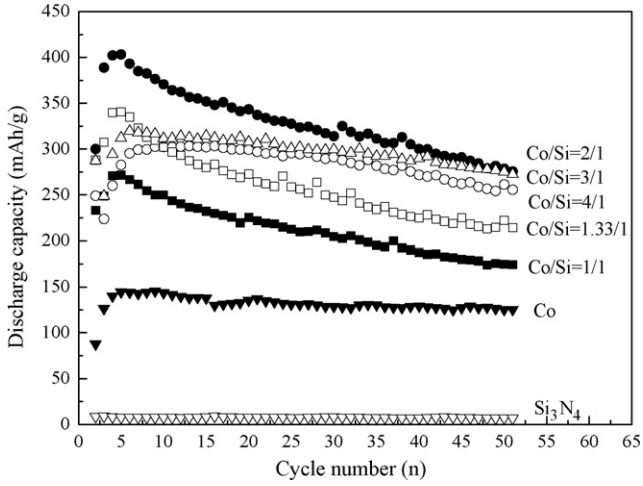

Fig. 3. Cycle performance of ball-milled Si_3N_4, Co and Co–Si_3N_4 composites.

all pre-charged samples in the first cycle. The discharge potential plateau in the first cycle for all samples is lower as compared with that of metal hydride electrodes.

The cycle performance of ball-milled Co, Si_3N_4 and Co–Si_3N_4 composites with different Co/Si molar ratios at the discharge current density of 60 mA g^{-1} is indicated in Fig. 3. It is clear that the amorphous Si_3N_4 powders are electrochemically inactive in alkaline solution. The electrochemical capacity of ball-milled pure Co sample is only 144 mAh g^{-1} after 5 cycles. It is demonstrated that there is an activation process and all Co–Si_3N_4 composites exhibit considerably larger reversible capacities as compared with the ball-milled Co sample. The discharging capacities of Co–Si_3N_4 composites vary with increasing the Co/Si molar ratio from 1/1 to 4/1. The addition of inactive Si_3N_4 here is to ensure the homogeneous distribution of active cobalt particles for obtaining large capacities. The higher fraction of active Co in the composites is favorable for improving the cycle stability of the composite electrode, because the cycle performance of composites with the Co/Si molar ratio of 3/1and 4/1 is similar to pure Co electrode, exhibiting a quite good capacity retention. It can be seen that the maximum reversible electrochemical capacity (403 mAh g^{-1}) of the Co–Si_3N_4 composites is obtained at the molar ratio of Co/Si = 2/1. According to a two-electron reaction process, the theoretical capacity of the Co redox is 909 mAh g^{-1} based on Faraday's law. The calculated effective capacity of the active metallic Co is 562 mAh g^{-1} after deduction of the mass contribution of Si_3N_4 powders. The utilization of the active metallic Co is 61.9% for the Co–Si_3N_4 composite with the molar ratio of Co/Si = 2/1. When excessive Co is involved in the composite, it seems that the agglomeration of the active Co particles becomes more serious, which leads to lower utilization of metallic Co. However, the high fraction of electrochemical inactive Si_3N_4 in the Co–Si_3N_4 composites results in a poor discharge capacity. Therefore, the composite with a Co/Si molar ratio of 2/1 shows the optimized electrochemical performance (including discharge capacity and cycle stability), which is used for further investigation of the microstructure and electrochemical performance in the following sections.

Typical TEM images of amorphous Si_3N_4 nanoparticles and ball-milled Co–Si_3N_4 composite (Co/Si = 2/1) are illustrated in Fig. 4. The Si_3N_4 amorphous matrix is observed clearly from the TEM image (Fig. 4a), in good agreement with the above XRD analysis. The cobalt nanoparticles with the size between 10 and 20 nm are well dispersed throughout the Si_3N_4 amorphous matrix as shown in Fig. 4b. The inactive Si_3N_4 matrix can ensure the high dispersion of Co nanoparticles by depressing the random conglomeration of nanoparticles during the high-energy ball-milling process. The formation of Co nanoparticles with a good reaction activity is responsible for the improved electrochemical performance of the Co–Si_3N_4 composites in alkaline solution.

In order to identify the surface chemical state of the as-prepared sample, Co 2p, Si 2p and N 1s core level spectra, before and after Ar^+ sputtering, were recorded in Fig. 5. The cobalt exists as CoO (780.2 eV) on the he surface of the ball-milled Co–Si_3N_4 composite before Ar^+ sputtering, due to the surface oxidation of active Co nanoparticles in air. After Ar^+

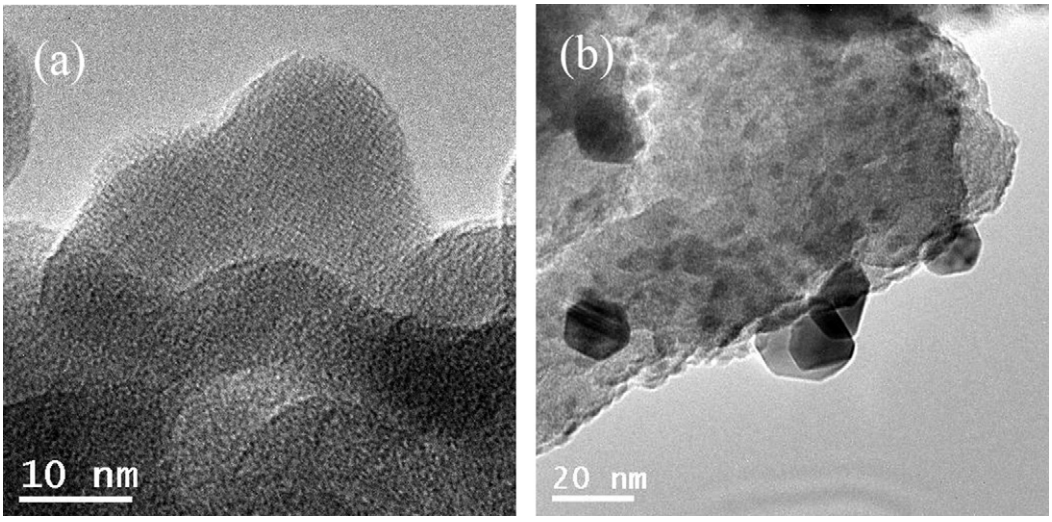

Fig. 4. TEM images of amorphous Si_3N_4 particles (a) and ball-milled Co–Si_3N_4 composite with the Co/Si molar ratio of 2/1 (b).

sputtering for 10 min, the characteristic Co 2p peak is shifted from 780.2 to 778.5 eV, suggesting the metallic Co exists the bulk phase in the composite. The binding energies of both N 1s and Si 2p almost remain the same value before and after Ar^+ sputtering, indicating the high-chemical stability of silica nitrides during the ball-milling process. The amorphous Si_3N_4 particles act only as the inactive matrix to support the highly dispersed active Co nanoparticles in the Co–Si_3N_4 composites, similar to the Co–BN composites [21].

The charge and discharge curves of Co–Si_3N_4 electrode with the Co/Si molar ratio of 2/1 at different cycles are displayed in Fig. 6. In the first cycle, the charge potential reaches to −1.02 V rapidly. The discharge potential plateau is around −0.74 V, and the discharge capacity is 300 mAh g^{-1} for the Co–Si_3N_4 composite. In the subsequent cycles, the charge potential plateau appears and polarization potential decreases during cycling, indicating an excellent charge acceptance. Meanwhile, the discharge potential plateau increases up to −0.80 V, and maintain the same value during cycling. To further confirm the electrochemical reaction process of the Co–Si_3N_4 electrode, cyclic voltammograms (CV) are presented in Fig. 7. In the first cycle, an oxidation peak appears around at the potential of −0.67 V (vs. HgO/Hg), corresponding to the low discharge potential plateau in the initial discharge process. In the second and third cycles, the oxidation peak shifts slightly to more negative potential (0.71–0.72 V), consistent with the increase of the discharge potential plateau. The couple of potential peaks in the cathodic and anodic processes suggest a reversible electrochemical reaction occurring on the Co–Si_3N_4 electrode. In the meantime, the integral area of the oxidation and cathodic peaks increases gradually with cycling, which is attributed to the existence of thin CoO layer on the surface of Co–Si_3N_4 composites.

Fig. 8 shows XRD patterns of the Co–Si_3N_4 composite with the Co/Si molar ratio of 2/1 at different charge and discharge states. At the fully charged state in the first cycle, XRD lines are consistent with the original sample, demonstrating that metallic Co is dominant in the Co–Si_3N_4 electrode before discharging.

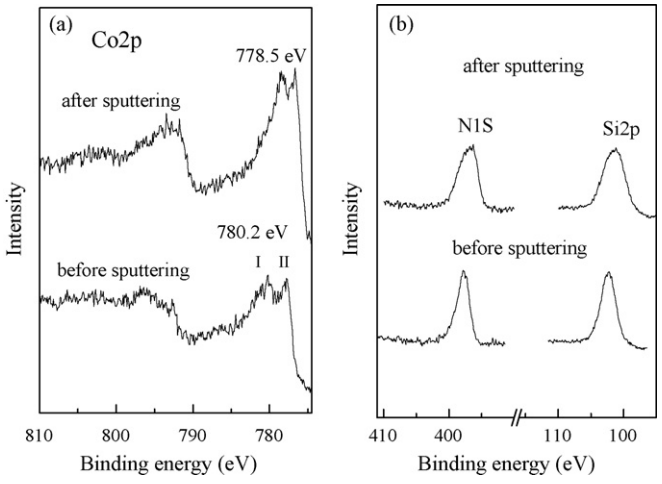

Fig. 5. Co 2p, Si 2p and N 1s core level spectra of the ball-milled Co–Si_3N_4 composite with the Co/Si molar ratio of 2/1 before and after Ar^+ sputtering for 10 min.

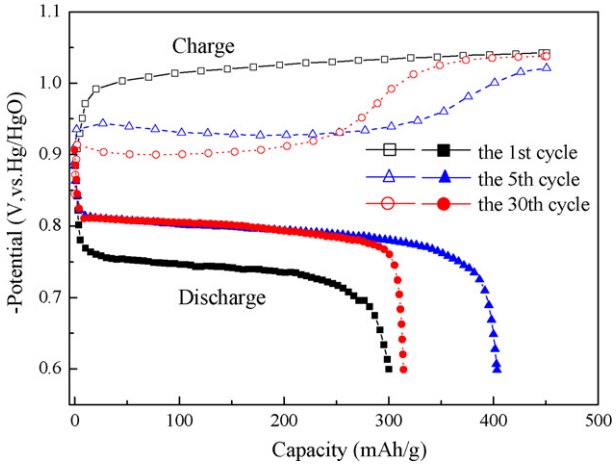

Fig. 6. Charge and discharge curves of Co–Si_3N_4 particles with the Co/Si molar ratio of 2/1 at different cycles. Open symbols are for charge curves and solid symbols are for discharge curves, respectively.

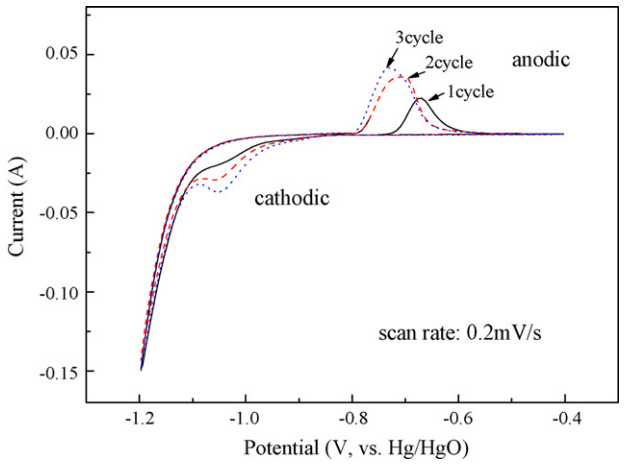

Fig. 7. Cyclic voltammograms of Co–Si_3N_4 particles with the Co/Si molar ratio of 2/1.

After discharging in the first cycle, most of the characteristic diffraction peaks can be indexed as β-$Co(OH)_2$ and the broad diffraction peaks of the metallic Co almost disappear. Similar phase transition can be repeated in the subsequent cycles. Moreover, the β-$Co(OH)_2$ phase is still detected as the coexisting phase with metallic Co at the fully charged state. It implies that the partial irreversible conversion between the active metallic Co and β-$Co(OH)_2$ is involved in the faradic reaction, resulting in the low utilization of metallic Co nanoparticles of the Co–Si_3N_4 composite as shown above.

The initial charge and discharge curves of the ball-milled $PrMg_{12}$–Ni composites with and without Co–Si_3N_4 composites (Co/Si = 2/1) are shown in Fig. 9, respectively. It can be clearly seen that the addition of Co–Si_3N_4 composites results in a notable enhancement of the initial discharge capacity. Moreover, the discharge potential plateau is extended in the range of −0.69 to −0.74 V, indicates that two electrochemical reaction processes of hydrogen electrochemical oxidation and Co redox reaction are involved for the $PrMg_{12}$–Ni composites with Co–Si_3N_4 as an additive. Further surface modification using Co-based composites with nanostructure is necessary for improving the electrochemical performance of hydrogen storage composites in future.

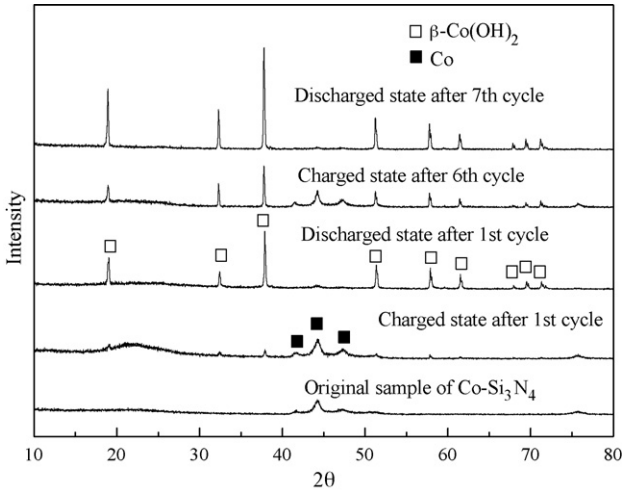

Fig. 8. XRD patterns of ball-milled Co–Si_3N_4 particles at different charge and discharge states (Co/Si molar ratio is 2/1).

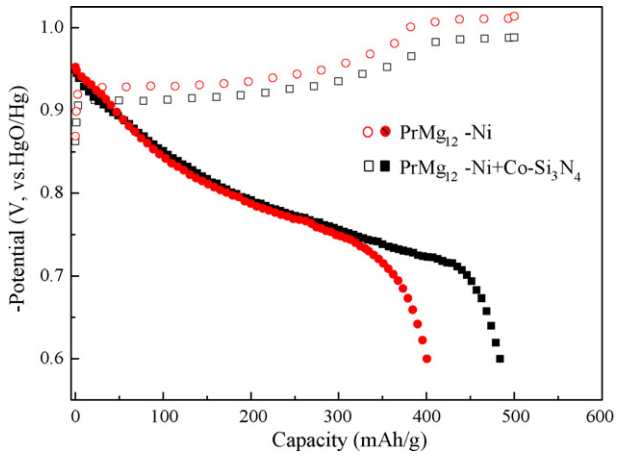

Fig. 9. The first charge and discharge curves of $PrMg_{12}$–Ni composites with and without the addition of Co–Si_3N_4 (14 wt%). Open symbols are for charge curves and solid symbols are for discharge curves, respectively.

4. Conclusion

The Co–Si_3N_4 composites are synthesized by ball-milling metallic Co and Si_3N_4 powder. It is found that metallic Co nanoparticles of 10–20 nm in size are highly dispersed on the amorphous inactive Si_3N_4 matrix after the ball-milling. The maximum discharge capacity (403 mAh g^{-1}) of the Co–Si_3N_4 composites is obtained at the molar ratio of Co/Si = 2/1. The formation of Co nanoparticles with a good reaction activity is responsible for the discharge capacity of the composites. The reversible faradic reaction between Co and β-$Co(OH)_2$ is dominant for ball-milled Co–Si_3N_4 composite. The surface modification of the hydrogen storage $PrMg_{12}$–Ni composites using Co–Si_3N_4 composites can enhance the initial discharge capacity based on the hydrogen electrochemical oxidation and Co redox reaction.

Acknowledgements

This work is supported by the 973 Program (2002CB211800) and NSFC (50671049), China.

References

[1] Q.D. Wu, X.P. Gao, G.R. Li, G.L. Pan, T.Y. Yan, H.Y. Zhu, J. Phys. Chem. C 111 (2007) 17082.
[2] J.N. Reimers, J.R. Dahn, J. Electrochem. Soc. 139 (1992) 2091.
[3] E.I. Santiago, L.C. Varanda, H.M. Villullas, J. Phys. Chem. C 111 (2007) 3146.
[4] M.D. Gross, J.M. Vohs, R.J. Gorte, Electrochim. Acta 52 (2007) 1951.
[5] S.R. Chung, K.W. Wang, T.P. Perng, J. Electrochem. Soc. 153 (2006) A1128.
[6] S.R. Chung, K.W. Wang, S.R. Sheen, C.T. Yeh, T.P. Perng, Electrochem. Solid-State Lett. 10 (2007) A155.
[7] Y.L. Cao, W.C. Zhou, X.Y. Li, X.P. Ai, X.P. Gao, H.X. Yang, Electrochim. Acta 51 (2006) 4285.

[8] Y.D. Wang, X.P. Ai, Y.L. Cao, H.X. Yang, Electrochem. Commun. 6 (2004) 780.
[9] Y.D. Wang, X.P. Ai, H.X. Yang, Chem. Mater. 16 (2004) 5194.
[10] G. He, L.F. Jiao, H.T. Yuan, Y.Y. Zhang, Y.J. Wang, Electrochem. Commun. 8 (2006) 1633.
[11] Y. Feng, L.F. Jiao, H.T. Yuan, M. Zhao, J. Alloys Compd. 440 (2007) 304.
[12] V. Brusic, G.S. Frankel, A.G. Schrott, T.A. Petersen, B.M. Rush, J. Electrochem. Soc. 140 (1993) 2507.
[13] L.P. Wang, Y.M. Lin, Z.X. Zeng, W.M. Liu, Q.J. Xue, L.T. Hu, J.Y. Zhang, Electrochim. Acta 52 (2007) 4342.
[14] P. Elumalai, H.N. Vasan, N. Munichandraiah, J. Power Sources 93 (2001) 201.
[15] A. Durairajan, B.S. Haran, B.N. Popov, R.E. White, J. Power Sources 83 (1999) 114.
[16] R.C. Ambrosio, E.A. Ticianelli, J. Electrochem. Soc. 150 (2003) E438.
[17] V. Pralong, A. Delahaye-Vidal, B. Beaudoin, J.B. Leriche, J.M. Tarascon, J. Electrochem. Soc. 147 (2000) 1306.
[18] T. Hayashi, S. Hirono, M. Tomita, S. Umemura, Nature 381 (1996) 772.
[19] X.N. Zhang, G.L. Pan, G.R. Li, J.Q. Qu, X.P. Gao, Solid State Ionics 178 (2007) 1107.
[20] Y. Wang, Z.W. Lu, Y.L. Wang, T.Y. Yan, J.Q. Qu, X.P. Gao, P.W. Shen, J. Alloys Compd. 421 (2006) 236.
[21] Z.W. Lu, S.M. Yao, G.R. Li, T.Y. Yan, X.P. Gao, Electrochim. Acta 53 (2008) 2369.